Vortex model and simulations for Rayleigh-Taylor and Richtmyer-Meshkov instabilities

Sung-Ik Sohn*
School of Information Engineering, Tongmyong University of Information Technology, Pusan 608-711, Republic of Korea
(Received 22 October 2003; published 30 March 2004)

The vortex method is applied to simulations of Rayleigh-Taylor (RT) and Richtmyer-Meshkov (RM) instabilities. The numerical results from the vortex method agree well with analytic solutions and other numerical results. The bubble velocity in the RT instability converges to a constant limit, and in the RM instability, the bubble and spike have decaying growth rates, except for the spike of infinite density ratio. For both RT and RM instabilities, bubbles attain constant asymptotic curvatures. It is found that, for the same density ratio, the RT bubble has slightly larger asymptotic curvature than the RM bubble. The vortex sheet strength of the RM interface has different behavior than that of the RT interface. We also examine the validity of theoretical models by comparing the numerical results with theoretical predictions.

DOI: 10.1103/PhysRevE.69.036703 PACS number(s): 83.85.Pt, 02.70.Pt, 47.20.Ma, 47.32.Cc

I. INTRODUCTION

The instability of an accelerated interface between fluids of different densities is a fundamental problem in fluid dynamics. The Rayleigh-Taylor (RT) instability occurs at an interface subject to gravitational acceleration [1] and the Richtmyer-Meshkov (RM) instability is driven by impulsive acceleration such as a shock wave [2]. Both instabilities play important roles in many fields ranging from astrophysics to inertial confinement fusion and are subjects of intensive current research.

Small perturbations at these unstable interfaces grow into nonlinear structures in the form of bubbles and spikes [3]. A bubble (spike) is a portion of the light (heavy) fluid penetrating into the heavy (light) fluid. At later times, a bubble in the RT instability attains a constant velocity, while a RM bubble has a decaying growth rate. Eventually, a turbulent mixing caused by vortex structures around spikes breaks the ordered fluid motion.

The RT and RM instabilities have been numerically studied by many people and various numerical methods have been applied to computations of complex unstable interfaces [4–17]. In this paper, we present numerical simulations for nonlinear evolutions of RT and RM instabilities by the point vortex method. In the point vortex method, the interface is considered as a set of point vortices and these vortices are computed in Lagrangian manner, without solving equations in whole two-dimensional grids [4,9]. This advantage of vortex method provides highly accurate and reliable solutions for unstable interfaces.

The numerical simulations for RT instability by the point vortex method were first performed by Baker *et al.* [4], and later by Kerr [9]. Kerr used the formulation based on the vortex dipole model. Tryggvason [7] and Zufiria [8] applied a different type of vortex method, so called vortex-in-cell method, to the RT instability. Rikanati *et al.* [15] reported the numerical results for RM instability for the limit of two fluids of same density ratio (Atwood number $A \rightarrow 0$) from the vortex model. In Ref. [15], they used the reduced model which placed only two opposite vortices at the middle of a bubble and spike. To the author's knowledge, the vortex methods have not been applied so far to the simulations of RM instability of finite density contrast. The main purpose of this paper is the numerical simulations for RT and RM instabilities from a full vortex model and the investigation of various aspects of dynamics for unstable interfaces.

Potential flow models for unstable interfaces have been recently developed by several authors [18–22] and analytic solutions for bubbles and spikes are obtained. We compare results from the vortex method with analytic solutions of potential flow models. The examination for the validity of potential flow models through quantitative comparisons of predictions from theoretical models with numerical results is also a key issue of this paper.

The point vortex method in our computations uses the formulation of the vortex model in Baker *et al.* [4]. However, the classical method in Ref. [4] has several difficulties in the implementations, so that modifications to the classical method are needed for stable computations. First of all, the vortex method in Ref. [4] suffers from the numerical instability, due to singularity, as the number of point vortices increases. From this reason, they focused mostly on the infinite density ratio case and the results for finite density ratios had low resolutions for the interfaces. To overcome the numerical instability from singularity, we adopt Krasny's method [23], which regularizes point vortices as vortices with finite cores or ''blobs'' of vortices. Krasny's desingularization method makes the point vortex method stable for large number of point vortices, so that it provides high resolutions of the interface. The additional difficulty is the development of steep profiles of vortex sheet strength at late times. To handle the shocklike behavior of vortex sheet strength, we apply the upwind (or, shock-capturing) method to computations of the equation for vortex sheet strength.

The vortex methods usually assume incompressible flows, while the RM instability occurs mostly in compressible fluids in reality. For compressible RM instability, the author and coworker showed that the unstable system transits from approximately linear and compressibility dominant stage to nonlinear and nearly incompressible stage [24]. Holmes *et al.* [16] have further examined the nonlinear theory in Ref.

*Present address: Department of Mathematics, Kangnung National University, Kangnung 210-702, Republic of Korea. Electronic address: sohnsi@kangnung.ac.kr

[24] and shown that the transition from linear compressible to potential flow is valid for the small amplitude initialization and weak to moderate shock strength. Therefore, even for compressible RM instability, driven by a weak or moderate shock, the vortex methods are relevant for most of time ranges except the early linear stage.

In Sec. II, we present the vortex model for the evolutions of stratified unstable interfaces and the numerical algorithm to solve the vortex model. The numerical results are presented in Sec. III for the RT instability and Sec. IV for the RM instability. Section V discusses the results and gives conclusion.

II. VORTEX METHOD

A. Vortex model

We consider an interface in a vertical channel filled with two fluids of different densities in two dimensions. Fluids are inviscid, incompressible, and irrotational, and the motion of fluids is governed by the Euler equation

$$\mathbf{a}_i = -\frac{1}{\rho_i}\nabla p_i - g\mathbf{j}, \quad i=1,2, \tag{1}$$

where $\mathbf{a}$ is the acceleration of a material particle, ρ density of fluid, p pressure in the fluid, g the external acceleration, and $\mathbf{j}$ a unit vector along y axis. From the potential flow assumption, the interface can be modeled as a vortex sheet [25]. The strength of vortex sheet γ is defined as the jump in the tangential velocities of two fluids across the interface

$$\gamma = (\mathbf{u}_1 - \mathbf{u}_2)\cdot\mathbf{s}. \tag{2}$$

Here, $\mathbf{u}_1$ and $\mathbf{u}_2$ are velocities below and above the interface, respectively, and $\mathbf{s}$ is the unit tangent vector at the interface.

The Lagrangian velocity of interface is expressed by

$$\mathbf{q} = \mathbf{U} + \tfrac{1}{2}\gamma\alpha\mathbf{s}, \tag{3}$$

where $\mathbf{U}$ represents the average of velocities on either side,

$$\mathbf{U} = \tfrac{1}{2}(\mathbf{u}_1 + \mathbf{u}_2), \tag{4}$$

and α, $|\alpha| \leqslant 1$, is the weighting parameter. Taking $\alpha = 1$, the vortices follow the lower fluid and, taking $\alpha = -1$, the vortices follow the upper fluid.

Since the interface velocity is a weighted average of fluid velocities at the interface, the parameter α in Eq. (3) indirectly determines the distribution of vortices along the interface. If the resolution of the interface is good overall, the results are independent of α. However, if the vortices are strongly clustered and the arclength of the interface is rapidly elongated in some regions, the results depend on α and the appropriate choice of α allows the computations to proceed to much longer time. The issue of choosing the numerical parameter α will be discussed later.

The interface is described by a parametric curve $\mathbf{x} = \mathbf{x}(s,t)$, with the arclength s and time t, and is evolved by

$$\frac{d\mathbf{x}}{dt} = \mathbf{q}. \tag{5}$$

The average velocity $\mathbf{U}$ is given by the Biot-Savart law

$$\mathbf{U}(s,t) = \frac{1}{2\pi}\int_{-\infty}^{\infty} \frac{\mathbf{k}\times[\mathbf{x}(s,t) - \mathbf{x}(\tilde{s},t)]}{|\mathbf{x}(s,t) - \mathbf{x}(\tilde{s},t)|^2}\gamma(\tilde{s},t)d\tilde{s}, \tag{6}$$

where the principal value integral is taken along the sheet and $\mathbf{k}$ is the unit vector normal to the two-dimensional plane for the fluid system. For the periodic boundary condition with period 2π, the Biot-Savart law (6) reduces to

$$u - \mathrm{i}v = \frac{1}{4\pi\mathrm{i}}\int_0^{2\pi}\tilde{\gamma}\cot\left(\frac{z-\tilde{z}}{2}\right)d\tilde{s}. \tag{7}$$

Here, u and v represent the horizontal and vertical components of the average velocity $\mathbf{U}$, and $z = x + \mathrm{i}y$ in complex notation, and $\tilde{\gamma} = \gamma(\tilde{s})$, $z = z(s)$, $\tilde{z} = z(\tilde{s})$.

An alternative way to the Biot-Savart law is the vortex-in-cell method [7,8], which evaluates the velocity field by solving the Poisson equation for the stream function in the whole domain. Note that the vortex-in-cell method has a smoothing for solutions by grid effects. The vortex method used in our study has a similar smoothing effect as the vortex-in-cell method when the regularization parameter is applied.

To determine the average velocity by Eq. (7), the evolution equation for the vortex sheet strength γ is needed. The acceleration $\mathbf{a}_i$ has the following kinematic relation:

$$\mathbf{a}_i = \frac{d\mathbf{u}_i}{dt} - \tfrac{1}{2}\gamma(\alpha \pm 1)\frac{\partial \mathbf{u}_i}{\partial s}, \tag{8}$$

where the $+(-)$ sign is for $i = 2(1)$. Subtracting the tangential component of Euler equations (1) of each fluid and using Eq. (8), we have

$$(\mathbf{a}_1 - \mathbf{a}_2)\cdot\mathbf{s} = A(\mathbf{a}_1 + \mathbf{a}_2)\cdot\mathbf{s} + 2Ag\mathbf{j}\cdot\mathbf{s} \tag{9}$$

$$= A\left(2\frac{d\mathbf{U}}{dt}\cdot\mathbf{s} + \frac{1}{4}\frac{\partial\gamma^2}{\partial s} - \gamma\alpha\frac{\partial\mathbf{U}}{\partial s}\cdot\mathbf{s}\right) + 2Ag\mathbf{j}\cdot\mathbf{s}, \tag{10}$$

where $A = (\rho_2 - \rho_1)/(\rho_2 + \rho_1)$ is the Atwood number. Then, by the relation (8), Eq. (10) becomes

$$\frac{d\gamma}{dt} = 2A\frac{d\mathbf{U}}{dt}\cdot\mathbf{s} + \frac{\partial}{\partial s}\left(\frac{\alpha + A}{4}\gamma^2 + 2Agy\right) - (1 + \alpha A)\gamma\frac{\partial\mathbf{U}}{\partial s}\cdot\mathbf{s}. \tag{11}$$

The Eqs. (5), (7), and (11) determine the evolution of vortex sheet between stratified fluids. Note that Eq. (11) is actually an integro-differential equation for γ, since $\mathbf{U}$ is coupled to γ by Eq. (7).

The external acceleration g is set to a constant for the Rayleigh-Taylor instability and 0 for the Richtmyer-

Meshkov instability. The Richtmyer-Meshkov interface is evolved by giving the initial velocity, which in turn is the approximation of the interface state resulting from the interaction of an incident shock wave and the interface.

B. Numerical method

The RT-type instability develops a singularity due to the roll-up around the spike and this produces a difficulty in numerical computations. To overcome this, we apply a desingularization parameter $\delta>0$ to Eq. (7) [23]. The "δ equations" for Eq. (7) are

$$u=-\frac{1}{4\pi}\int_0^{2\pi}\frac{\sinh(y-\tilde{y})}{\cosh(y-\tilde{y})-\cos(x-\tilde{x})+\delta^2}\tilde{\gamma}\ d\tilde{s}, \quad (12)$$

$$v=\frac{1}{4\pi}\int_0^{2\pi}\frac{\sin(x-\tilde{x})}{\cosh(y-\tilde{y})-\cos(x-\tilde{x})+\delta^2}\tilde{\gamma}\ d\tilde{s}. \quad (13)$$

To solve the system of equations numerically, we discretize the interface $\{\mathbf{x}_i\}_{i=0}^N$ and the vortex sheet strength $\{\gamma_i\}_{i=0}^N$ where N is the number of point vortices. Given $\{\mathbf{x}_i\}$ and $\{\gamma_i\}$, the velocity field can be evaluated from Eqs. (3), (12), and (13). Applying direct summations for the integral, Eqs. (12) and (13) are approximated by

$$u_i=-\frac{1}{4\pi}\sum_{j\neq i}\Gamma_j\frac{\sinh(y_i-y_j)}{\cosh(y_i-y_j)-\cos(x_i-x_j)+\delta^2}, \quad (14)$$

$$v_i=\frac{1}{4\pi}\sum_{j\neq i}\Gamma_j\frac{\sin(x_i-x_j)}{\cosh(y_i-y_j)-\cos(x_i-x_j)+\delta^2}. \quad (15)$$

Here, Γ_i represents the local circulation, defined as

$$\Gamma_i=\gamma_i\ \Delta s_i, \quad (16)$$

where Δs_i is the segment of arclength,

$$\Delta s_i=\tfrac{1}{2}\sqrt{(x_{i+1}-x_{i-1})^2+(y_{i+1}-y_{i-1})^2}.$$

The interface position and vortex sheet strength in time are determined by Eqs. (5) and (11)–(13). For time integrations of these coupled equations, we apply an iteration method. The numerical procedures of time integrations are described as follows: Assuming that the discrete position $\mathbf{x}_i^n$, the average velocity $\mathbf{U}_i^n$ and the vortex sheet strength γ_i^n are given at current time step n, we first estimate $d\gamma_i^n/dt$ by Eq. (11) with $d\mathbf{U}_i^{n-1}/dt$ at previous time step. Then, we update γ_i^{n+1} and advance the interface by Eq. (5) with Eq. (3), by suitable time stepping methods. Using the updated values for the interface position and vortex sheet strength, the velocity field at next time step, $\mathbf{U}_i^{n+1}$, is evaluated from Eqs. (14) and (15). Then, we can compute the new estimate for $d\mathbf{U}_i^n/dt$ by the central difference with respect to time, i.e.,

$$\frac{d\mathbf{U}_i^n}{dt}=\frac{\mathbf{U}_i^{n+1}-\mathbf{U}_i^{n-1}}{2\Delta t}. \quad (17)$$

Initially, $d\mathbf{U}_i^n/dt$ is updated by the forward difference, $d\mathbf{U}_i^n/dt=(\mathbf{U}_i^{n+1}-\mathbf{U}_i^n)/\Delta t$. This iteration procedure is repeated until convergence. In our computations, six iterations are needed, on average, to achieve convergence for given tolerance 10^{-8}. Note that, for the integration of time stepping, the trapezoidal method is applied for the interface and Euler's method for the vortex sheet strength.

In the computation of Eq. (11), we apply central differences for $\mathbf{s}, \partial y/\partial s$ and $\partial\mathbf{U}/\partial s$. However, the discretization of the term in γ^2 in Eq. (11) should be carefully taken. As time proceeds, the vortex sheet strength develops a complicated structure and becomes very steep around the center of roll up at the spike. This shocklike behavior of vortex sheet strength is due to the term in γ^2, because this term makes Eq. (11) a type of Burgers equation. Discretizations based on central difference for $\partial\gamma^2/\partial s$ are numerically unstable and the computations stop when the profile becomes steep.

The similarity of Eq. (11) to Burgers equation suggests the use of the upwind method [26] for the term γ^2. Here, we apply the Godunov method, which is the simplest upwind method. The Godunov method approximates the term $F=-\gamma^2$ at the midpoints between vortices by

$$F_{i+1/2}=\max[(\gamma_i^+)^2,\ (\gamma_{i+1}^-)^2], \quad (18)$$

where

$$\gamma^+=\max(-\gamma,0), \quad \gamma^-=\min(-\gamma,0). \quad (19)$$

This formulation based on the upwind difference provides stable computations for Eq. (11), so that it runs much longer time than methods based on central differences. Note that the upwind method was first applied to the computation of vortex sheet by Zufiria [8].

It has been found that point vortices on the interface tend to migrate away from the spike region toward the bubble, so that the spike is poorly resolved at late times. In our computations, the nonuniform distribution of point vortices is controlled by the weighting parameter α in Eq. (3). As mentioned earlier, the parameter α indirectly determines the distribution of vortices along the interface, without changing the solution itself. We have found that the choice $\alpha=-A^2$ is effective for our simulations and gives good resolution for the interface. This choice of α was also used by Kerr [9] for the computation of Rayleigh-Taylor instability by the method based on vortex dipole model.

C. Initial conditions

To apply the described numerical algorithm to unstable interfaces, the position and the vortex sheet strength of all vortex points should be given initially. In this paper, we focus on the evolutions of initial sinusoidal interface in the channel of width 2π,

$$z=a_0\cos(x). \quad (20)$$

For the Rayleigh-Taylor instability, $\gamma_i=0$ for all vortex points, assuming that the initial velocity of the interface is 0.

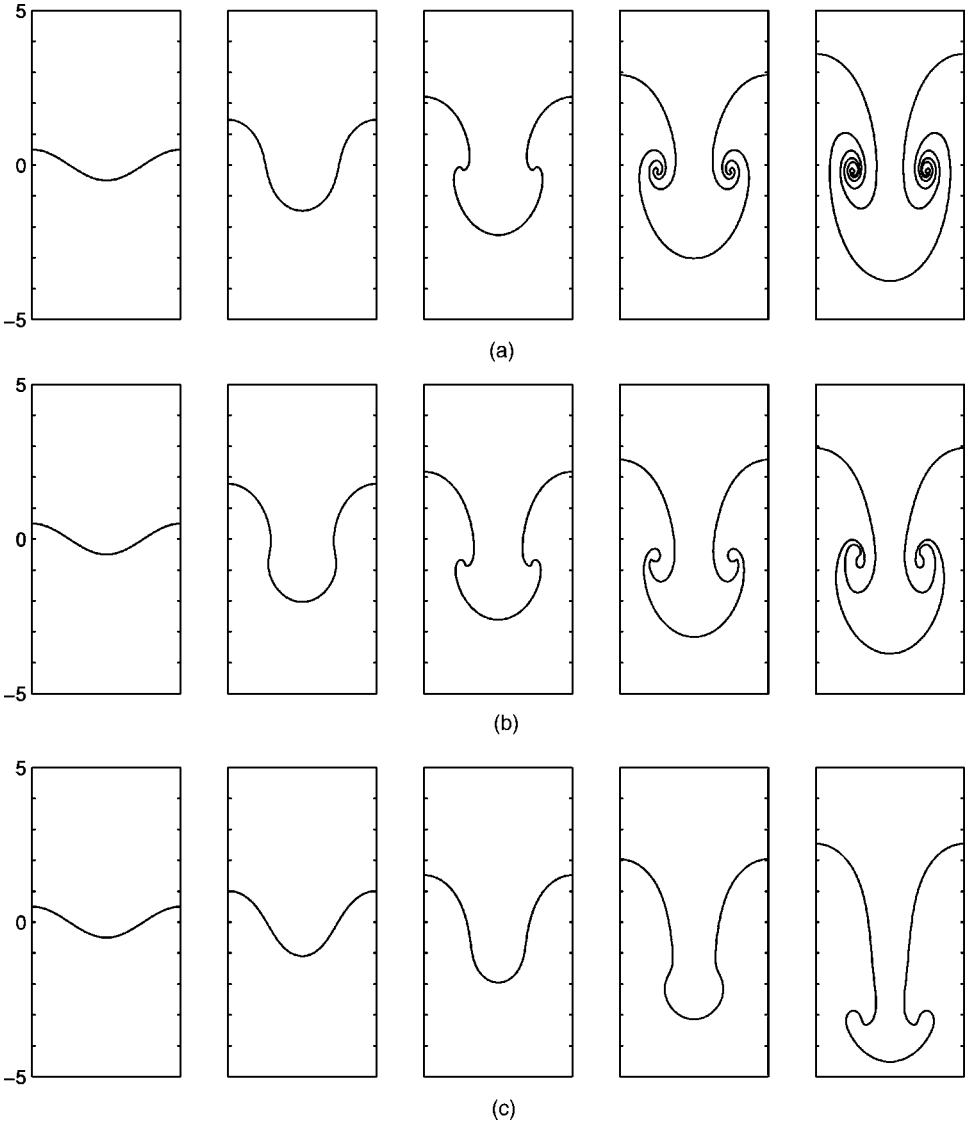

FIG. 1. Evolutions of RT instability. Atwood numbers are (a) $A=0.05$, (b) $A=0.3$, (c) $A=0.7$. Times are (a) $t=0$, 10, 14, 18, 22, (b) $t=0$, 5, 6, 7, 8, (c) $t=0$, 2, 3, 4, 5.

For the Richtmyer-Meshkov instability, the initial condition for vortex sheet strength can be obtained from the theoretical model. We take the velocity potential ansatz

$$\phi_1=\nu_0 e^{y}\cos x, \quad \phi_2=-\nu_0 e^{-y}\cos x \tag{21}$$

for lower and upper fluid, respectively. The velocity potential ansatz (21) comes from the Richtmyer impulsive model [2] and is typically used in the modeling of RM instability [24,27]. From this velocity potential ansatz, the initial condition for local circulations in RM instability is given by

$$\Gamma_i=-\nu_0(x_{i+1}-x_{i-1})\sin x_i \cosh y_i . \tag{22}$$

The vortex sheet strengths are determined from Eq. (16).

The initial velocity along vortex points is given by Eqs. (14) and (15). If the parameter δ is 0, ν_0 in Eq. (22) defines the initial velocity of the RM bubble and spike. In our computations, $\delta>0$ is used for finite density ratio cases, so that the initial velocity of the bubble and spike is smaller than ν_0. For infinite density ratio case, we use $\delta=0$, because the interface of $A=1$ has a smooth profile without roll-up and a regularization is not needed.

III. RESULTS FOR RAYLEIGH-TAYLOR INSTABILITY

We apply the described numerical algorithm of the vortex method and perform numerical experiments for the nonlinear evolutions of Rayleigh-Taylor instability. For all computations, the gravitational acceleration is set to $g=1$ and the number of vortex points $N=400$.

All results in this section are plotted in dimensionless units. The dimensionless length, time, and velocity are given by $k\mathbf{x}$, $t\sqrt{kg}$, and $\mathbf{U}\sqrt{k/g}$, respectively, where $k=2\pi/L$ is the wave number and L is the channel width.

Figure 1 illustrates the results for evolutions of RT unstable interfaces for chosen Atwood numbers, $A=0.05$, 0.3, and 0.7 (density ratios 1:1.105, 1:1.857, and 1:5.667, respectively). The initial amplitude of perturbed interface is $a_0=0.5$. The computational time steps are $\Delta t=0.002$ for $A=0.05$, and $\Delta t=0.001$ for $A=0.3$ and 0.7. The regulariza-

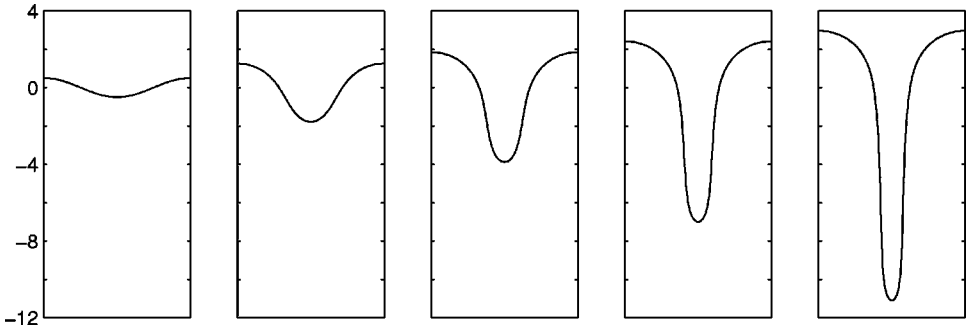

FIG. 2. Evolution of RT instability for $A=1$. Times are $t=0$, 2, 3, 4, and 5.

tion parameter is set to $\delta=0.15$. We see from Fig. 1 that the spike has stronger roll-up for smaller Atwood number and the difference of amplitudes of the bubble and spike at late times becomes large as the Atwood number increases.

The result for the case of infinite density ratio, $A=1$, is displayed in Fig. 2. The regularization parameter is set to $\delta=0$, for the reason mentioned previously. The initial amplitude of interface is $a_0=0.5$ and the time step $\Delta t=0.001$.

Figure 3 plots the bubble and spike velocities for the results of Figs. 1 and 2. For comparisons, theoretical predictions for the asymptotic bubble velocity from the potential flow model [21] are also shown by dashed lines. The author [21] has recently generalized Layzer's potential flow model [28], originally for infinite density ratio, to the system of arbitrary density ratio and obtained the analytic solution for the asymptotic velocity and curvature of the RT bubble,

$$v_{\mathrm{bb}} \rightarrow \sqrt{\frac{Ag}{(2+A)k}}, \quad |\xi_{\mathrm{bb}}| \rightarrow \frac{k}{3}. \tag{23}$$

Figure 3 shows that the numerical results for the bubble velocity agree well with the analytic solution (23).

To show the dependence of the regularization parameter δ, we compare the results for various values of δ. Figure 4 shows the bubble and spike velocities for $\delta=0.1$, 0.15, and 0.2 for the system of $A=0.3$. Figure 4 shows that the velocity field grows slightly faster for smaller value of δ, but converges to quantitatively similar values. The computations with $\delta=0.1$ are stopped around $t=7.3$ due to lack of resolution. Figure 5 is the comparison of RT unstable interfaces of $A=0.3$ for $\delta=0.1$, 0.15, and 0.2 at time $t=7$. We see that the resolution of the spike is refined as δ decreases and the amplitudes of the bubble and spike are slightly larger for smaller value of δ.

Figure 6 is the bubble curvatures for $A=0.05$, 0.3, 0.7, and 1.0 with initial amplitudes $a_0=0.3$ and 0.5. In Fig. 6, the sign of the bubble curvature is changed for plot. The bubble curvatures converge to values between 0.5 and 0.55, forgetting initial amplitudes. The asymptotic bubble curvatures for

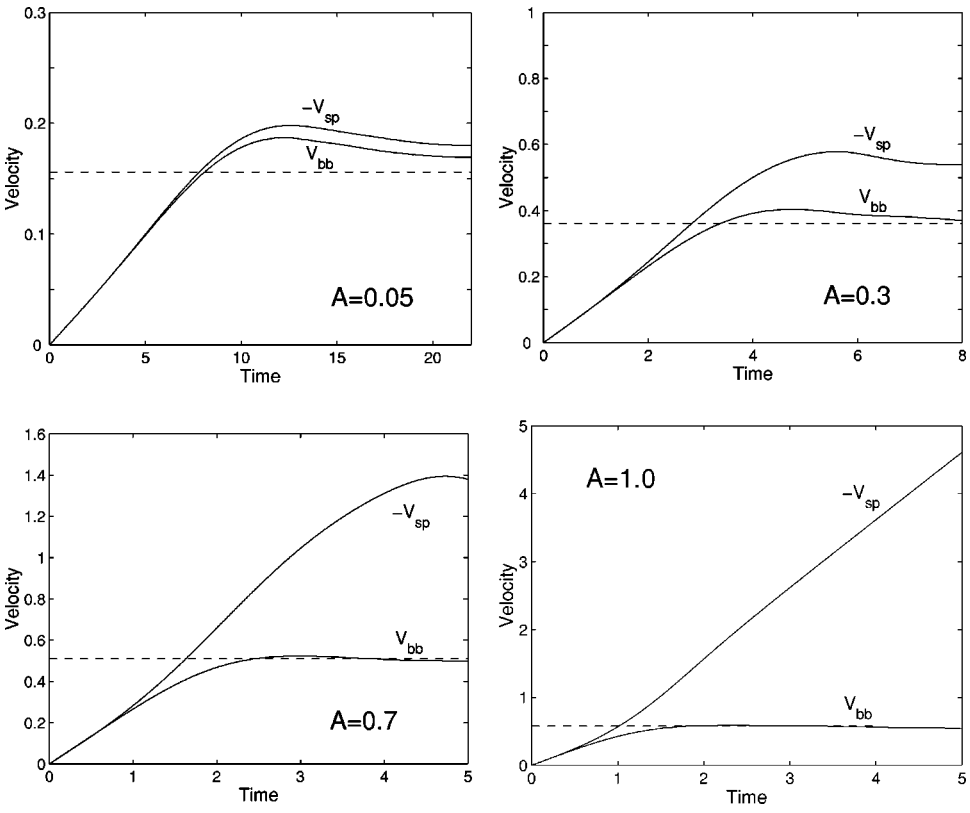

FIG. 3. Bubble and spike velocities of RT instability for $A=0.05$, 0.3, 0.7, and 1.0. The solid curves are results from the vortex method and the dashed lines are theoretical predictions for asymptotic bubble velocity from the potential flow model.

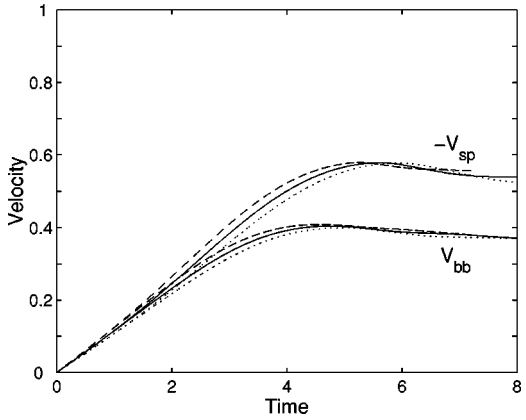

FIG. 4. Comparison of bubble and spike velocities of RT instability for various values of regularization parameter δ. The Atwood number is $A=0.3$. The dashed curve corresponds to $\delta=0.1$, the solid curve to $\delta=0.15$, and the dotted curve to $\delta=0.2$.

$A=0.3$ and 0.7 are larger than that for $A=0.05$ and $A=1$. Therefore, it seems that the asymptotic bubble curvature is not monotonic with respect to the Atwood number.

The theoretical prediction (23) from the Layzer-type potential flow model gives 1/3 for the asymptotic bubble curvature in this case, which has a range of difference from 34% to 40% with the numerical results. The reason for this relatively large difference is that the analytic solution (23) is derived from the approximate modeling and the curvature is a much more sensitive parameter than the velocity. The predictions from the theoretical model can be improved by providing more appropriate form of potential to the model. Zufiria [29] proposed a different potential flow model, applying a potential with singularity. Note that Layzer's model uses an analytic potential. The asymptotic solution for the RT bubble in Zufiria's model is

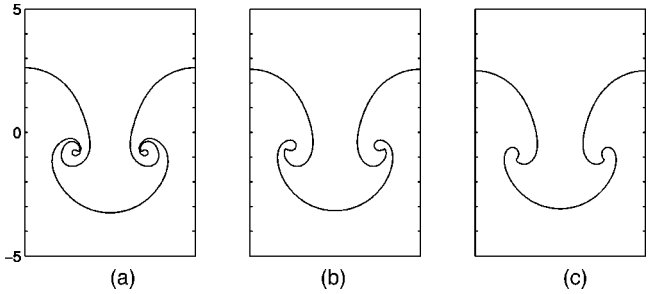

FIG. 5. Comparison of evolutions of RT unstable interfaces for various values of regularization parameter δ at time $t=7$. The Atwood number is $A=0.3$ and the number of vortex points is $N=400$. (a) $\delta=0.1$, (b) $\delta=0.15$, (c) $\delta=0.2$.

$$\nu_{bb}\rightarrow 0.963\sqrt{\frac{g}{3k}}, \quad |\xi_{bb}|\rightarrow\frac{k}{\sqrt{3}}, \tag{24}$$

which is given by Sohn and Zhang [19]. The solution (24) is valid only for $A=1$ and Zufiria's model still has not been extended to general $A<1$. The solution (24) predicts 0.577 for the asymptotic bubble curvature in this case, which has about 15% difference with the numerical result for $A=1$. The prediction for the asymptotic bubble velocity from Eq. (24) has little difference with that from Layzer's model or numerical results.

Figure 7 is the distribution of vortex sheet strengths along the RT interfaces for the results of Figs. 1 and 2 at selected

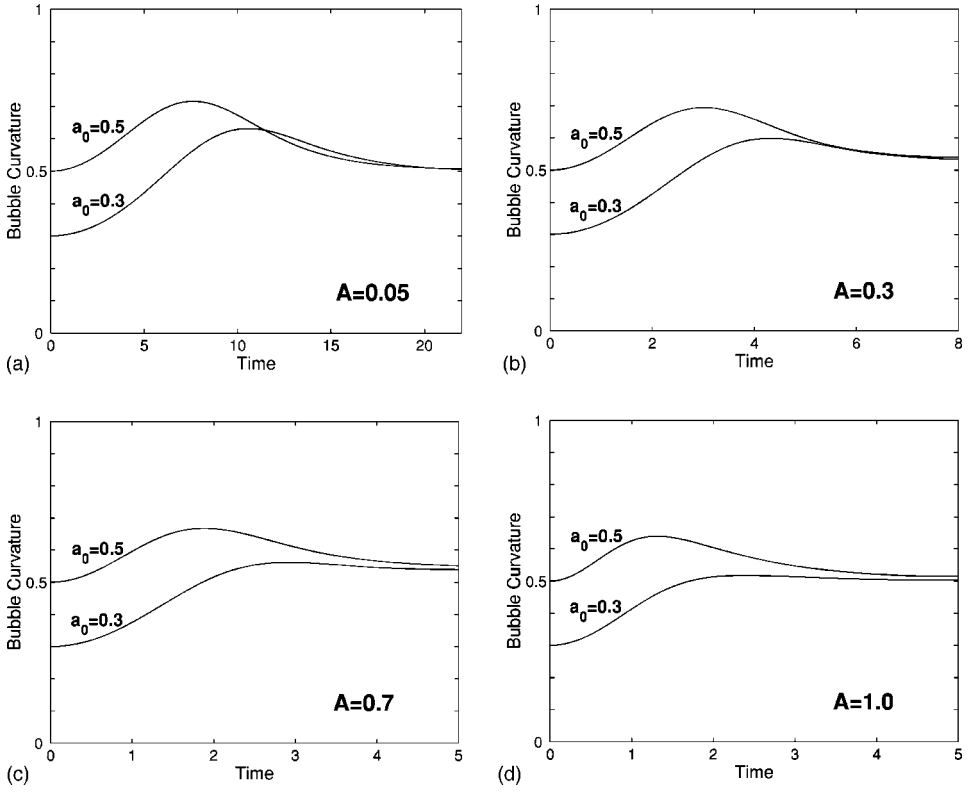

FIG. 6. Bubble curvatures of RT instability with initial amplitudes $a_0=0.3$ and 0.5. Atwood numbers are (a) $A=0.05$, (b) $A=0.3$, (c) $A=0.7$, (d) $A=1$.

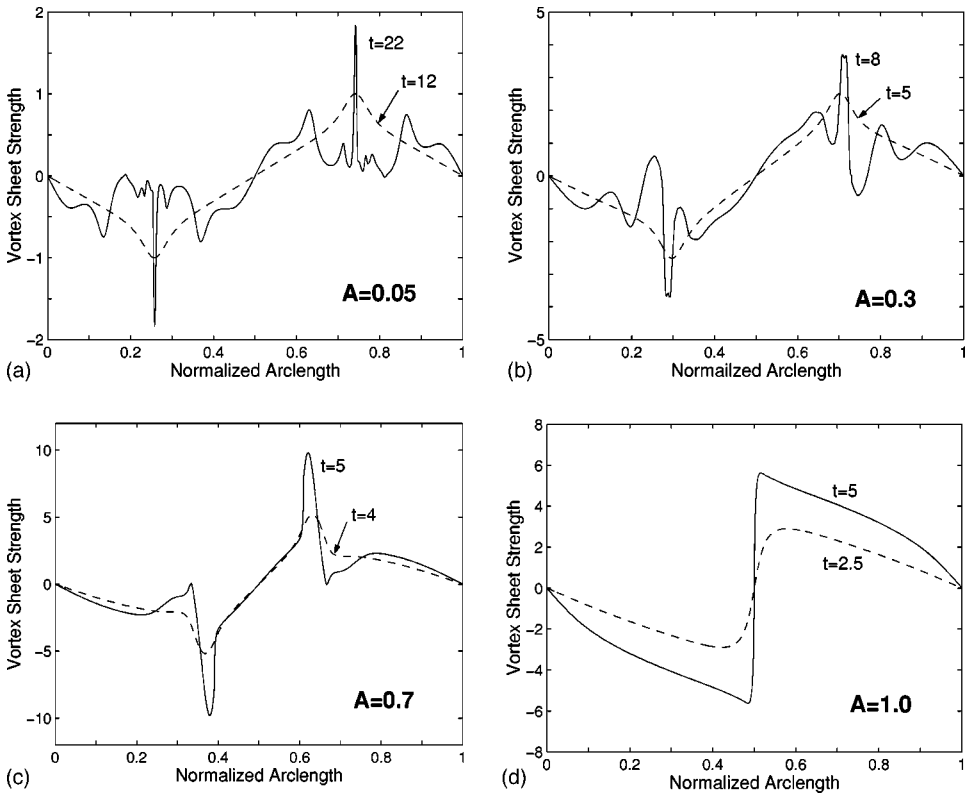

FIG. 7. Distributions of vortex sheet strengths along RT interfaces. Atwood numbers are (a) $A=0.05$, (b) $A=0.3$, (c) $A=0.7$, (d) $A=1$.

times. The x axis represents the normalized arclength. We observe that the vortex sheet strength tends to be narrow around the time of formation of spike and has more complicated structure at late times for smaller value of Atwood number. The vortex sheet strength for $A=0.05$ is almost symmetric with respect to vortex peaks, due to weak density stratification of the system. Note that the vortex sheet strength for the system of $A=0$ is symmetric with respect to vortex peaks [7]. Figure 7(d) shows that the vortex sheet strength for $A=1$ becomes single shocklike profile at late times.

IV. RESULTS FOR RICHTMYER-MESHKOV INSTABILITY

In this section, we present the numerical results for Richtmyer-Meshkov instability from the vortex method. The number of vortex points is set to $N=400$ for all computations, except results for finer vortices in Fig. 10.

For RM instability, we choose units typically used in shock-tube experiments [30]. The units can be rescaled by $\mathbf{U}\rightarrow s_1\mathbf{U}$, $\mathbf{x}\rightarrow s_2\mathbf{x}$, $t\rightarrow(s_2/s_1)t$.

Figure 8 illustrates the results for evolutions of RM unstable interfaces for finite density ratio cases. We choose the Atwood numbers, $A=0$, 0.3, and 0.7. The initial amplitude is $a_0=0.5$ cm and the initial velocity of the bubble and spike is 0.8 cm/ms, by setting $\nu_0=1$ cm/ms in Eq. (22) and $\delta=0.15$. The computational time steps are $\Delta t=0.001$ ms for all cases. Figure 8 shows that, similarly as the RT instability, the RM interface has stronger roll-up for smaller Atwood number. We also observe that, for smaller Atwood number, the amplitude of the RM bubble is larger at later times and that of the RM spike is smaller.

The result for the case of infinite density ratio, $A=1$, is displayed in Fig. 9. The regularization parameter is set to $\delta=0$. The initial amplitude of the interface is $a_0=0.5$ cm and the initial interface velocity is 0.8 cm/ms, directly setting $\nu_0=0.8$ cm/ms in Eq. (22). The computational time step is taken as $\Delta t=0.0005$ ms.

We validate the present method by comparing our results with other numerical results. Figure 10 shows the comparison of results from the vortex method for bubble and spike velocities with the results obtained by Menikoff and Zemach [5]. Menikoff and Zemach applied the method of conformal mapping for the RT instability and, to extend the model to the RM instability, set $g=0$ and gave nonzero initial velocity for the interface, which is the same approach as given in this paper. In both results, the same initial conditions, $a_0=0$ (flat interface) and $\nu_0=0.5$ cm/ms, are used. The solid curves are the results from the vortex method and the circles from the method of conformal mapping in Ref. [5]. We performed simulations using finer vortices, $N=200$, 400, and 800. We see the convergence of our results to the spike velocity obtained by the conformal mapping and perfect agreements for the bubble velocity. The results from the vortex method for the bubble velocity are identical for all cases. Note that the comparison of results for the RT instability from the point vortex method and the method of conformal mapping is given in Baker *et al.* [4].

The bubble and spike velocities for the results of Figs. 8 and 9 are plotted in Fig. 11. The velocities of bubbles and spikes decay to zero for all cases, except the spike of $A=1$. For smaller Atwood number, the growth rate of the bubble is larger, while that of the spike is smaller. The dashed curves in Fig. 11(a) are theoretical predictions for

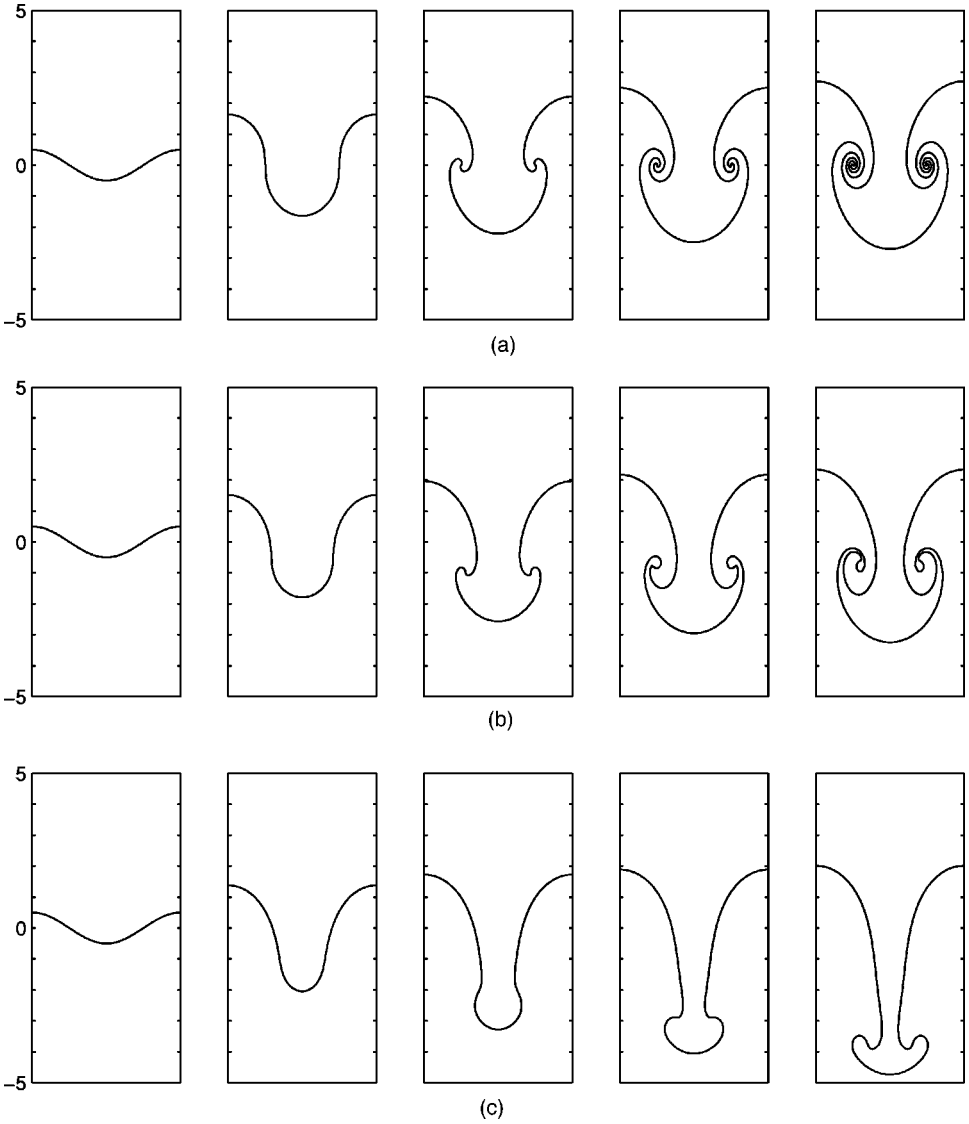

FIG. 8. Evolutions of RM instability. Atwood numbers are (a) $A=0$, (b) $A=0.3$, (c) $A=0.7$. The initial interface velocity is 0.8 cm/ms. Times are $t=0$, 2, 4, 5.5, and 7 ms for each case. The domain is $[0,2\pi]\times[-5,5]$ cm^2.

asymptotic growth rates of bubbles from the Layzer-type potential flow model [21]. The asymptotic solution for the RM bubble in Ref. [21] is

$$v_{\mathrm{bb}} \sim \frac{2}{(2+A)kt}, \quad |\xi_{\mathrm{bb}}| \rightarrow \frac{k}{3}. \tag{25}$$

For all cases, the numerical results for the bubble velocity fit well with the theoretical prediction. The dashed line in Fig. 11(b) is the theoretical prediction for the asymptotic spike velocity for $A=1$ from the Layzer model, which is obtained by Zhang [18]. The asymptotic solution for the RM spike of $A=1$ in Zhang [18] is

$$v_{\mathrm{sp}} \rightarrow v_0 \left(\frac{3\xi_0+3}{3\xi_0+1} \right)^{1/2}, \quad \xi_{\mathrm{sp}} \rightarrow \infty, \tag{26}$$

where $\xi_0=\xi(t=0)$. Figure 11(b) shows that the numerical

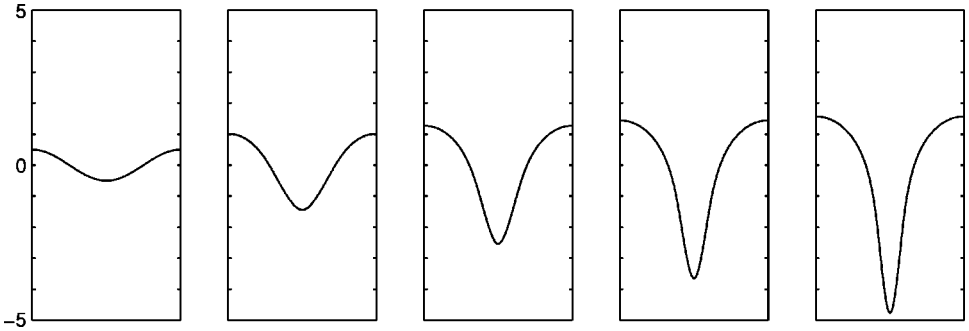

FIG. 9. Evolution of RM instability for $A=1$. The initial interface velocity is 0.8 cm/ms. Times are $t=0$, 1, 2, 3, and 4 ms. The domain is $[0,2\pi]\times[-5,5]$ cm^2.

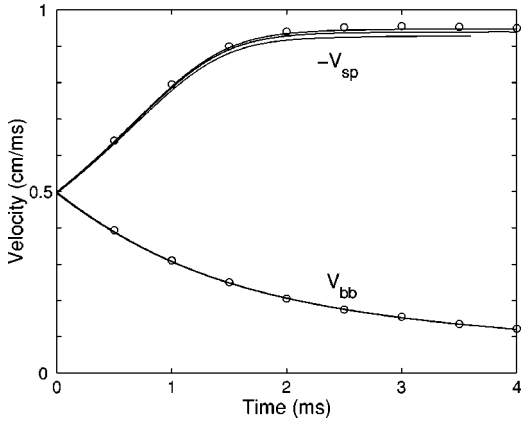

FIG. 10. Comparison of present results with other numerical results for $A=1$. The solid curves are results from the vortex method with $N=200$, 400, and 800. The circles correspond to results from the method of conformal mapping in Ref. [5]. The initial conditions are $a_0=0$ (flat interface) and $\nu_0=0.5$ cm/ms.

result for the spike velocity is in good agreement with the analytic solution. For the case of Fig. 10 (flat interface), the solution (26) gives 0.866 cm/ms, which is in reasonable agreement with the numerical results.

Figure 12 shows the bubble curvatures for the results of Figs. 8 and 9, and the results with the initial amplitude $a_0=0.3$ cm. The bubble curvatures converge to values between 0.45 and 0.5 cm^{-1}, independent of initial amplitudes. We again do not find a monotone behavior of the asymptotic bubble curvature with respect to the Atwood number. It is interesting to compare the results of RM bubble curvatures with the RT cases. For the same Atwood number, the asymptotic curvature of the RM bubble is slightly smaller than that of the RT bubble.

The asymptotic curvature (25) for the RM bubble from Layzer's model is same as that for the RT bubble and has a range of difference from 27% to 34% with the numerical results. On the other hand, the asymptotic solution for the RM bubble of $A=1$ from Zufiria's model [19] is

$$\nu_{\mathrm{bb}}\sim\frac{0.6}{kt},\quad |\xi_{\mathrm{bb}}|\rightarrow\frac{k}{2.61}. \tag{27}$$

In Zufiria's model, the RT bubble has larger asymptotic curvature than the RM bubble. This behavior for the bubble curvature in Zufiria's model is consistent with the numerical results. The solution (27) gives 0.383 cm^{-1} for the asymptotic bubble curvature in our case, which has about 15% difference with the numerical result for $A=1$ and is in better agreement with the numerical result than Layzer's model. The prediction for the asymptotic bubble velocity from the solution (27) is slightly lower than that from Layzer's model and also fits better with the numerical result.

Figure 13 plots the vortex sheet strengths along the RM interfaces for the results of Figs. 8 and 9 at selected times. The vortex sheet strength of the RM unstable interface for $A=0$ is symmetric with respect to vortex peaks and is concentrated at midpoints of the bubble and spike. The structure of vortex sheet strength for the RM interface of $A=0$ is much simpler than that of weakly stratified RT instability in Fig. 7(a). The single shocklike behavior of vortex sheet strength for $A=1$ in Fig. 13(d) is similar to the RT case of $A=1$ in Fig. 7(d). However, the peak of vortex sheet strength for the RM instability of $A=1$ does not increase with respect to time, unlike the RT case of $A=1$.

We mentioned in Sec. I that Rikanati *et al.* [15] used the reduced vortex model for $A=0$ which gave only two opposite vortices at the middle of the bubble and spike. The concentration of the vortex sheet strength at midpoints of the bubble and spike, in Fig. 13(a), shows that the assumption used in Ref. [15] is indeed reasonable. Moreover, this behavior supports the agreement of the analytic solution for asymptotic bubble velocity for $A=0$ from the reduced vortex model [Eq. (7) in Ref. [15]] and the solution (25) from the potential flow model.

V. DISCUSSION AND CONCLUSIONS

We have presented the numerical simulations for RT and RM instabilities by the vortex method. The numerical results show that the vortex method has been successfully applied to the nonlinear evolutions of unstable interfaces.

The point vortex method used in our computations has provided highly resolved solutions for unstable interfaces. The regularization parameter δ is applied for stable computations and, for smaller value of δ, the roll up of the spike is refined. The computations with very small δ have serious troubles at late times and we showed that the magnitude of δ has small effect on the solutions of physical variables.

The dynamics of unstable interfaces have been thoroughly

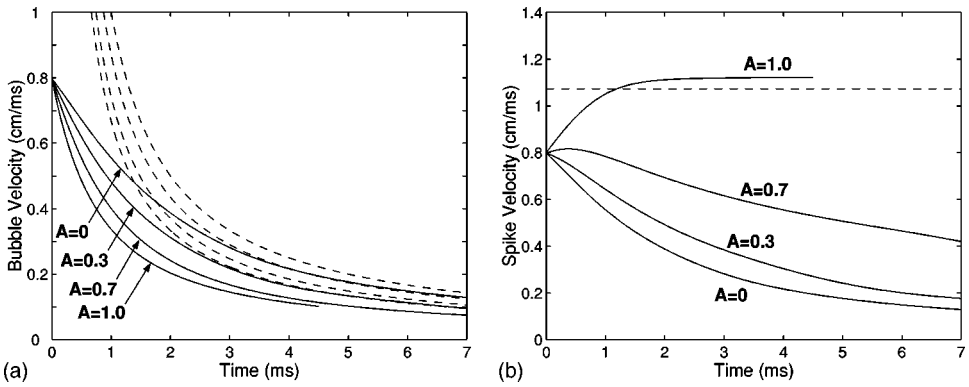

FIG. 11. Bubble and spike velocities of RM instability for Atwood numbers $A=0$, 0.3, 0.7, and 1. The dashed curves in (a) are the theoretical predictions for the asymptotic growth rate of bubbles for $A=0$, 0.3, 0.7, and 1 from above to below. The dashed line in (b) is the theoretical prediction for the asymptotic spike velocity of $A=1$.

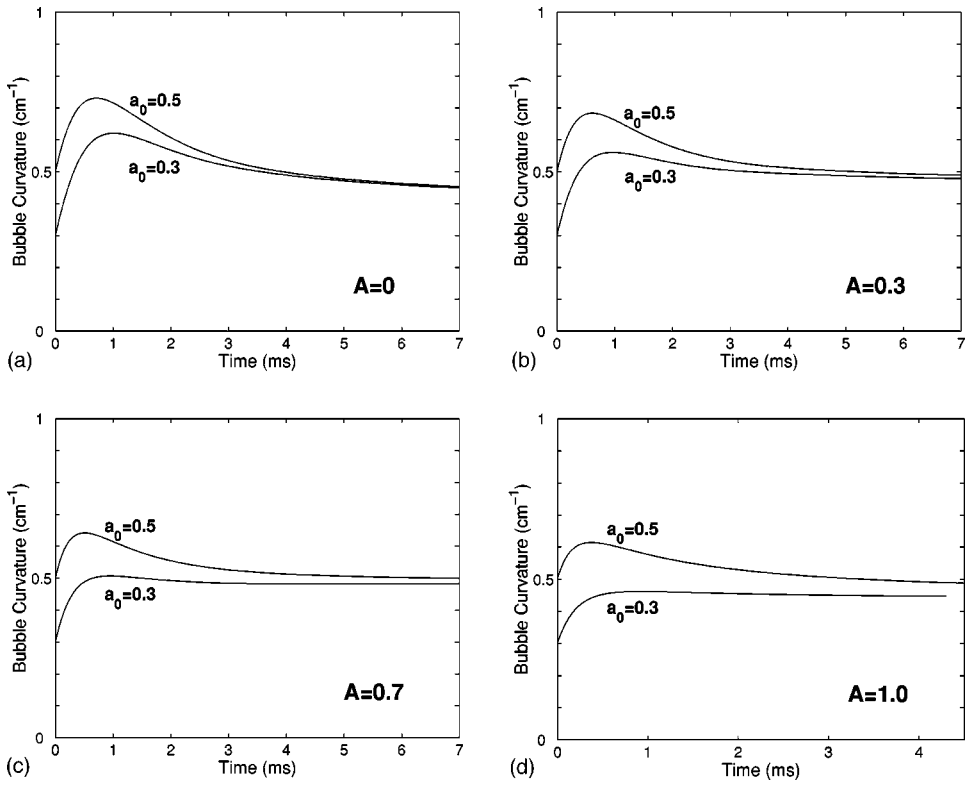

FIG. 12. Bubble curvatures of RM instability with initial amplitudes $a_0=0.3$ and 0.5 cm. Atwood numbers are (a) $A=0$, (b) $A=0.3$, (c) $A=0.7$, (d) $A=1$.

investigated by the vortex method. The results for bubble and spike velocities quantitatively agree with the analytic solutions of potential flow models. The RT bubble attains a constant asymptotic velocity, which is proportional to the Atwood number for fixed gravitational acceleration and geometric parameters. In the RM instability, the bubble and spike have decaying growth rates, except that the spike of $A=1$ converges to a constant asymptotic velocity. Fixing physical parameters, the growth rate of the RM bubble is larger for smaller Atwood number, while that of the RM

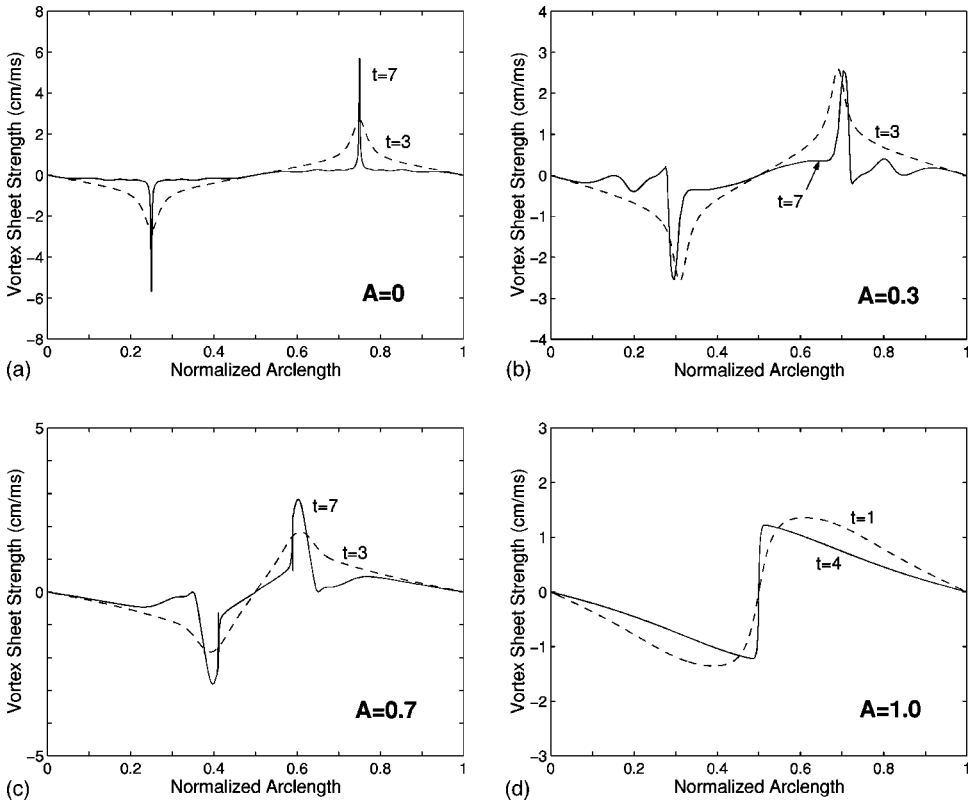

FIG. 13. Distributions of vortex sheet strengths along RM interfaces. Atwood numbers are (a) $A=0$, (b) $A=0.3$, (c) $A=0.7$, (d) $A=1$.

spike is smaller.

The RT and RM bubbles have constant asymptotic curvatures, independent of initial amplitudes. We have found that, for the same Atwood number, the RT bubble has slightly larger asymptotic curvature than the RM bubble. It seems that, for both RT and RM instabilities, the asymptotic bubble curvature is not monotonic with respect to the Atwood number.

The studies on bubble curvatures have raised the issue for validity of theoretical models. The predictions for asymptotic bubble curvatures, as well as asymptotic bubble velocities, from Zufiria's potential flow model agree better with the numerical results than Layzer's model. The quantitative differences between two models for predictions for solutions come from the choice of potential function in the models. The Layzer model uses a sinusoidal form of potential and the Zufiria model has more sophisticated potential which is derived from complex conformal mapping. Therefore, one may conclude that the Zufiria model is more appropriate for unstable interfaces than the Layzer model. The advantage of Layzer's model is in the simple form of potential, so that it has been generalized to the system of arbitrary density ratio in several ways. The Zufiria model is still limited to the case of infinite density ratio and its extension to general cases has not been established yet.

The numerical results show that the vortex sheet strengths of RT and RM interfaces have different behaviors. In the RT instability, the vortex sheet strength has more complex structures as the Atwood number decreases. For the RM instability of $A=0$, the concentration of vortex strength on the middle of the bubble and spike indicates that the reduced modeling, imposing only two vortices of different sign, is a reasonable approximation to the full model. The vortex sheet strength for the RM interface of $A=1$ becomes a single shocklike profile, but the peak of vortex strength does not grow at late times.

The vortex simulation for the turbulent mixing by initial multimode interactions is an interesting subject. For computations of fully developed or strongly interacting interfaces, the lack of resolution from nonuniform distribution of vortex points causes a serious loss of accuracy. Therefore, it should be handled by auxiliary procedures such as a redistribution or point insertion method. The application of the vortex method with a redistribution and/or point insertion procedure to fully developed interfaces and simulations of turbulent mixings of RT and RM instabilities are under the current research.

ACKNOWLEDGMENT

This work was supportd by Grant No. R01-2000-00002 from the Basic Research Program of the Korea Science and Engineering Foundation.

[1] G.I. Taylor, Proc. R. Soc. London, Ser. A **201**, 192 (1950).
[2] R.D. Richtmyer, Commun. Pure Appl. Math. **13**, 297 (1960).
[3] D. Sharp, Physica D **12**, 3 (1984).
[4] G.R. Baker, D.I. Meiron, and S.A. Orszag, Phys. Fluids **23**, 1485 (1980).
[5] R. Menikoff and C. Zemach, J. Comput. Phys. **51**, 28 (1983).
[6] D.L. Youngs, Physica D **12**, 32 (1984); Laser Part. Beams **12**, 725 (1994).
[7] G. Tryggvason, J. Comput. Phys. **75**, 253 (1988); H. Aref and G. Tryggvason, Phys. Rev. Lett. **62**, 749 (1989).
[8] J.A. Zufiria, Phys. Fluids **31**, 3199 (1988).
[9] R.M. Kerr, J. Comput. Phys. **76**, 48 (1988).
[10] J.F. Hawley and N.J. Zabusky, Phys. Rev. Lett. **63**, 1241 (1989).
[11] J. Glimm, R. Menikoff, X.L. Li, D.H. Sharp, and Q. Zhang, Phys. Fluids A **2**, 2046 (1990).
[12] L.D. Cloutman and M.F. Wehner, Phys. Fluids A **4**, 1821 (1992).
[13] R.L. Holmes, J.W. Grove, and D.H. Sharp, J. Fluid Mech. **301**, 51 (1995).
[14] C. Mügler and S. Gauthier, Phys. Rev. E **58**, 4548 (1998).
[15] A. Rikanati, U. Alon, and D. Shvarts, Phys. Rev. E **58**, 7410 (1998).
[16] R.L. Holmes, G. Dimonte, B. Fryxell, M.L. Gittings, J.W. Grove, M. Schneider, D.H. Sharp, A.L. Velikovich, R.P. Weaver, and Q. Zhang, J. Fluid Mech. **389**, 55 (1999).
[17] J. Glimm, J.W. Grove, X.L. Li, and D.C. Tan, SIAM J. Sci. Comput. (USA) **21**, 2240 (2000); J. Glimm, J.W. Grove, and Y.M. Zhang, *ibid.* **24**, 208 (2002).
[18] Q. Zhang, Phys. Rev. Lett. **81**, 3391 (1998).
[19] S.-I. Sohn and Q. Zhang, Phys. Fluids **13**, 3493 (2001).
[20] V.N. Goncharov, Phys. Rev. Lett. **88**, 134502 (2002).
[21] S.-I. Sohn, Phys. Rev. E **67**, 026301 (2003).
[22] K.O. Mikaelian, Phys. Rev. E **67**, 026319 (2003).
[23] R. Krasny, J. Comput. Phys. **65**, 292 (1986).
[24] Q. Zhang and S.-I. Sohn, Phys. Lett. A **212**, 149 (1996); Phys. Fluids **9**, 1106 (1997).
[25] P. G. Saffman, *Vortex Dynamics* (Cambridge University Press, New York, 1992).
[26] R. J. LeVeque, *Numerical Methods for Conservation Laws* (Birkhäuser, Basel, 1992).
[27] J.W. Jacobs and J.M. Sheeley, Phys. Fluids **8**, 405 (1996).
[28] D. Layzer, Astrophys. J. **122**, 1 (1955).
[29] J. Zufiria, Phys. Fluids **31**, 440 (1988).
[30] A.N. Aleshin, E.V. Lazareva, S.G. Zaitsev, V.B. Rozanov, E.G. Gamalii, and I.G. Lebo, Sov. Phys. Dokl. **35**, 159 (1990); M. Brouillette and B. Sturtevant, Phys. Fluids A **5**, 916 (1993).